paring its performance to that obtained with a mirror based on rectangular holes. It has been shown that the new design outclasses the traditional one, both in terms of plane-wave reflection loss and impact on the feed radiation pattern.

REFERENCES

1. B.A. Munk, Frequency selective surfaces: Theory and design, Wiley Interscience, New York, 2000.
2. P. Besso, M. Bozzi, L. Perregrini, L. Salghetti Drioli, and W. Nickerson, Deep space antenna for rosetta mission: design and testing of the S/X-band dichroic mirror, IEEE Trans Antenn Propag 51 (2003), 388–394.
3. M. Bozzi, L. Perregrini, J. Weinzierl, and C. Winnewisser, Efficient analysis of quasi-optical filters by a hybrid MoM/BI-RME method, IEEE Trans Antenn Propag 49 (2001), 1054–1064.
4. P. Besso, M. Bozzi, M. Formaggi, S. Germani, M. Pasian, and L. Perregrini, Innovative approach for the design of a S/X/Ka-band dichroic mirror for ESA deep space antenna DSA1, in 28th ESA Antenna Workshop on Space Antenna Systems and Technologies, ESA/ESTEC, Noordwijk, The Netherlands, May 31–June 3, 2005.
5. J.C. Chen, Computation of reflected and transmitted horn radiation patterns for a dichroic plate, TDA Progress Report 42–119, Jet Propulsion Lab, Pasadena, CA (1994), 236–254.

MICROMACHINED INTERDIGITAL FILTER ON SILICON

Neil Thomson and Jia-Sheng Hong
Department of Electrical, Electronic and Computer Engineering, Heriot-Watt University, Edinburgh EH14 4AS, The United Kingdom

Received 2 March 2006

ABSTRACT: *This article presents a microwave interdigital filter manufactured on high resistive silicon substrate. Two filter designs are referenced in this article; both filters are five pole interdigital filters with one using uniform impedance resonators and the other using stepped impedance resonators. The fabrication of the filters on silicon has been possible with the use of micromachining. This therefore enables filters to be manufactured with smaller footprints and gives rise to further development with micro-electro-mechanical systems technology.* © 2006 Wiley Periodicals, Inc. Microwave Opt Technol Lett 48: 1862–1866, 2006; Published online in Wiley InterScience (www.interscience.wiley.com). DOI 10.1002/mop.21810

Key words: *microwave filters; interdigital filters; micromachining; silicon*

1. INTRODUCTION

The requirements for smaller microwave filters with higher performance in all microwave systems are increasing. The footprint of microwave filters is determined not only by the filter topology but also by the dielectric substrate. The configurations of the resonators play a key role in the size of the filter with some filter topologies requiring tighter coupling. Interdigital filters have been proposed [1, 2], due to small spacing required for coupling between resonators with larger bandwidths; substrates with low dielectric constants have been used. This results in a small compact filter design. The use of stepped impedance resonators (SIR) over the conventional uniform impedance resonators (UIR) designs has reduced the size of the interdigital filter further but has meant that high precision is now required for the fabrication. The high precision is provided by the use of surface micromachining [3, 4].

Using high resistive silicon substrate has enabled design of small band-pass filters for defence applications. Using the micromachining techniques has also given rise to further development in filter size reduction. The use of this technology has meant that integration with other silicon components on the same wafer is now possible. Integration of the device with other micro-electromechanical system (MEMS) components such as RF MEMS switches and varactors for switch filter banks and tuneable filters. Further reduction in size of the resonators has also been investigated by using bulk micromachining [5] to reduce the thickness of the silicon substrate directly below the capacitive element (low impedance section) on a step impedance resonator and profiling the ground plane. This leads to an increase in capacitance and a further reduction on the filter footprint.

TABLE 1 ***K*-Coefficients for the Design UIR Interdigital Filter with Symmetric Coupled Lines**

K_{12}	0.224
K_{23}	0.165
K_{34}	0.165
K_{45}	0.224

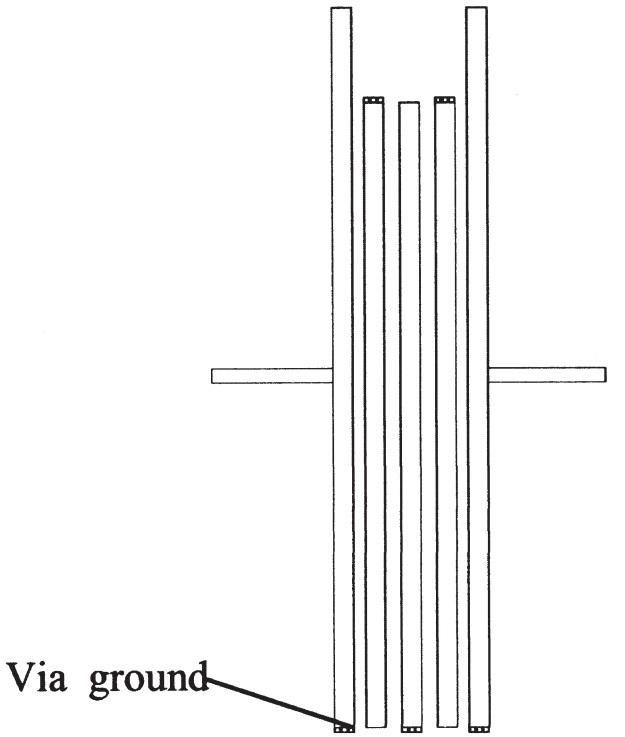

Figure 1 Designed UIR interdigital filter layout

2. FILTER DESIGN

The two symmetric interdigital filters were designed to be fabricated using silicon micromachining. The specification of the two filters is identical with one filter using conventional UIR. The second filter uses SIR and is mapped from the conventional UIR interdigital design; this is to reduce the overall footprint. The five pole filter design was chosen for its simplicity in design and would also effectively demonstrate the performance between the two filter designs.

The design specification for the given filter design used in this article requires a FBW of 33% at a center frequency of 1.5 GHz. This can be generally considered as having a large FBW. For our demonstration, the filter uses the Chebyshev lowpass prototype

TABLE 2 Dimensions of the Design UIR Interdigital Filter

Symmetric line width	0.5 mm
Input/output resonator lengths	20.45 mm
Remaining resonator lengths	17.75 mm
Spacing between resonator 1 and 2	0.3 mm
Spacing between resonator 2 and 3	0.4 mm
Length of tap point from via ground	10.0 mm

with a passband ripple of 0.04321 dB. The element g-values for the lowpass prototype are $g_0 = g_6 = 1.0$, $g_1 = 0.9714$, $g_2 = 1.3721$, $g_3 = 1.8014$, $g_4 = g_2$, and $g_5 = g_1$. For a conventional interdigital filter, the coupling coefficients K between coupled resonators i and $i + 1$ are defined by

$$K_{i,i+1} = \frac{Z_{0ei,i+1} - Z_{0oi,i+1}}{Z_{0ei,i+1} + Z_{0oi,i+1}}, \tag{1}$$

where $Z_{0ei,i+1}$ and $Z_{0oi,i+1}$ denote the even- and odd-mode impedances of coupled uniform lines. The K-coefficients can be easily calculated from the given lowpass prototype [2] and the results for the designed UIR interdigital filter with symmetric coupled lines are summarized in Table 1. These K-coefficients are then used in determining the layout (see Fig. 1) for the designed filter based on the desired even- and odd-mode impedances. The filter dimensions on a high resistive silicon substrate with a dielectric constant of 11.9 and a thickness of 0.525 mm are listed in Table 2. The simulated performance of the filter shown in Figure 2 matched the requirements given for the filter. The simulation was done using commercially available electromagnetic (EM) simulation software (Sonnet Software Inc., Release 10.52, Liverpool, NY), and the material (conductor and dielectric) losses have been taken into account.

To design the SIR filter, a new approach was adopted. The conventional design approach described previously was based on even- and odd-modes of coupled uniform lines and hence could not be used directly. On the other hand, for narrow-band filter designs, one may employ the well-known method based on the design parameters obtained as

$$Q_{el} = \frac{g_0 g_1}{\text{FBW}} \, Q_{en} = \frac{g_n g_{n+1}}{\text{FBW}}$$

$$M_{i,i+1} = \frac{\text{FBW}}{\sqrt{g_i g_{i+1}}} \text{ for } i = 1 \text{ to } n - 1, \tag{2}$$

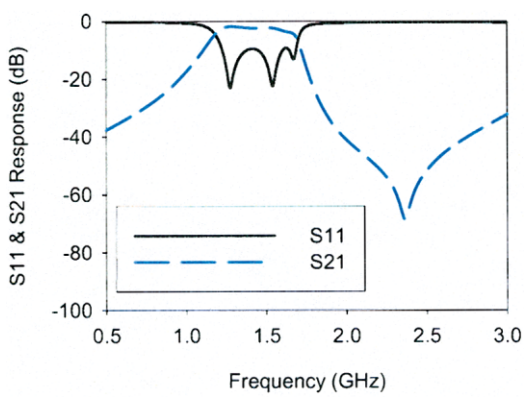

Figure 2 Simulated UIR interdigital filter response. [Color figure can be viewed in the online issue, which is available at www.interscience.wiley.com]

TABLE 3 Design Parameters Based on Eq. (2) for FBW = 0.33

Q_{el}	2.944
M_{12}	0.286
M_{23}	0.210
M_{34}	0.210
M_{45}	0.286

where g denotes the g-values for lowpass prototype, Q_{el} and Q_{en} are the external quality factors of the resonators at the input and output. $M_{i,i+1}$ are the coupling coefficients between the resonators. If we use the same lowpass prototype, we would have a set of design parameters from Eq. (2), which are listed in Table 3.

The main advantage of using Q and M design parameters lies in that it can be applied to any form of resonators, of course including the SIR. However, this approach is only valid for narrow-band filters, particularly for the fractional bandwidth below 10% for an accurate design. For our case, the required FBW is 33% and therefore, the above design parameters obtained based on Eq. (2) could not be used. To this end, a practical approach for designing SIR wide-band interdigital filters is described as later.

The conventional design using UIR plays a part in the design of the SIR interdigital filter. The UIR design is broken down, so simulation measurements can be taken to obtain a new set of design parameters. These results form a base for designing the SIR interdigital filter.

Each pair of the coupled resonator in the conventional design is modeled in EM software (Sonnet Software Inc., Release 10.52, Liverpool, NY). The typical coupling response of S_{21} is shown in Figure 3. Using the formulation of Eq. (3), a new set of coupling coefficients $M'_{i,i+1}$ can then be found, as listed in Table 4. The first resonator with input tap point is also modeled to find the external Q factor

$$M' = \frac{f_2^2 - f_1^2}{f_2^2 + f_1^2}. \tag{3}$$

When compared with Table 3, it is self-evident that the narrow-band approach for wideband SIR interdigital filter design could not be adopted directly. In particular, the external Q in Table 3 is larger than that in Table 4 by more than 45%, which would result

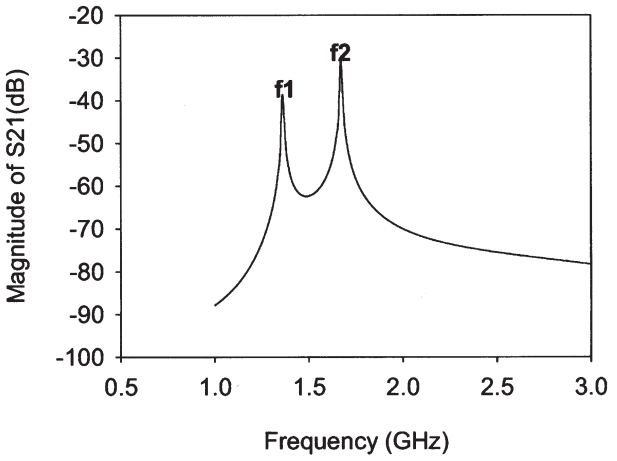

Figure 3 Typical coupling response between two λ/4 interdigital resonators

TABLE 4 New Design Parameters for SIR Interdigital Filter with FBW = 0.33

Q'_{e1}	2.03
M'_{12}	0.301
M'_{23}	0.207
M'_{34}	0.207
M'_{45}	0.301

in a narrower bandwidth. Hence emphasizes that the technique described in this article had to be adopted.

With the new set of design parameters obtained in Table 4, the Q' and M' parameters can easily be extracted from EM simulations so as to determine all the dimensions of the SIR interdigital filter. The dimensions of the SIR interdigital filter on the same silicon substrate are shown in Figure 4. The SIR design was then modeled in the simulation software (Sonnet Software Inc., Release 10.52, Liverpool, NY). The simulated results are plotted in Figure 5, showing a good match to the frequency response in Figure 2.

EM simulations were also carried out to investigate the loss effects on the SIR interdigital filter due to conductor, dielectric, and radiation respectively. Figure 6 shows the simulated results, where frequencies are normalized by the center frequency. Each curve shows the passband response when only one loss mechanism was considered. To simulate the conductor loss, 3-μm thick aluminum (as fabricated) with a conductivity of 3.72×10^7 S/m was assumed. To consider the dielectric loss in the simulation, a dielectric loss tangent of 0.01 for the high resistive silicon substrate was used. From Figure 6, one can see that the conductor loss is still dominant in this miniature filter. The loss from the silicon substrate is also significant, whereas the radiation loss is negligible.

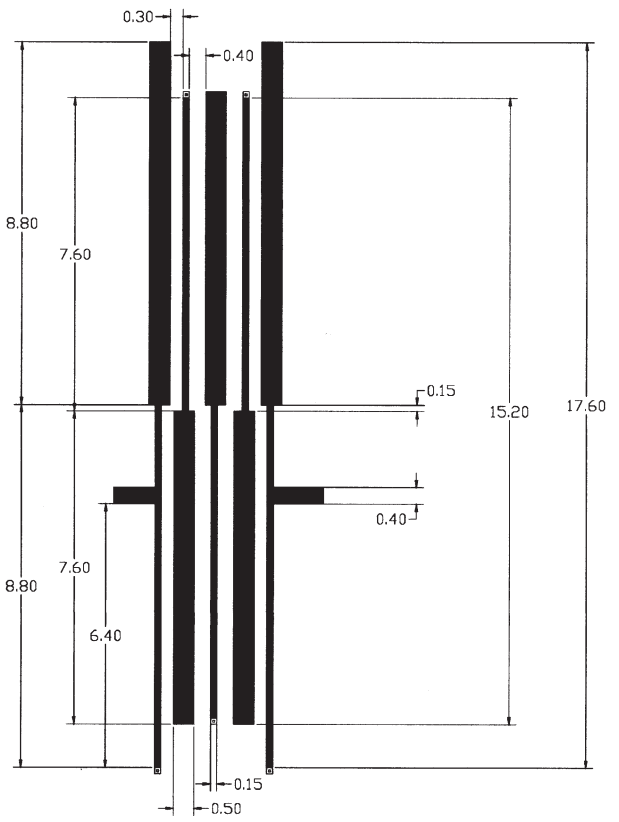

Figure 4 Dimensions (in millimeters) of interdigital filter with SIR

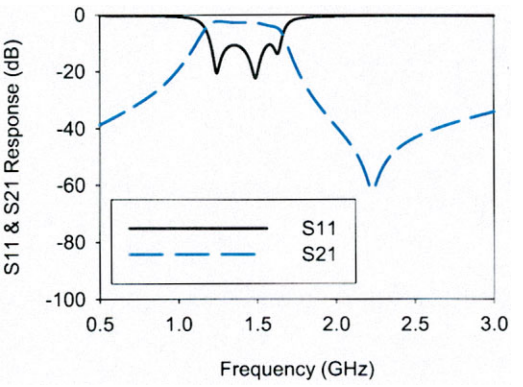

Figure 5 Simulated SIR interdigital filter response. [Color figure can be viewed in the online issue, which is available at www.interscience.wiley.com]

3. FABRICATION AND MEASUREMENT RESULTS

Fabrication of the interdigital filters was then carried out on high resistive silicon (>8 kΩ cm) and masks were laid out for 100 mm diameter wafers. The conductor and ground plane thickness were specified as 3 μm of aluminum. Aluminum was chosen as the conductor because this is the standard foundry metal. Standard IC fabrication techniques were used to pattern the conductor layers with deep reactive ion etching used to via down to the ground plane. Vias holes were metalised with aluminum and have been subsequently tested for good conductivity. A flash layer of gold 0.5 μm was also applied to the ground plane to ensure low resistance contact to the test housing. The test pieces were diced and mounted on brass test fixture using epoxy bond as shown in Figure 7 for a fabricated SIR interdigital filter.

The filters were tested using a HP microwave network analyzer. The measured results are given in Figures 8 and 9 for the UIR and SIR interdigital filters respectively. When compared with the simulated results from the EM modeling software, a good agreement can be observed. The FBW of the measured filters was recorded as 33 and 32% respectively. The design requirement was for 33% FBW so the filters have demonstrated that they match with the given specification. The measured wideband responses of both the UIR and SIR interdigital filters are shown in Figure 10. This highlights one of the additional properties of the SIR; it is its

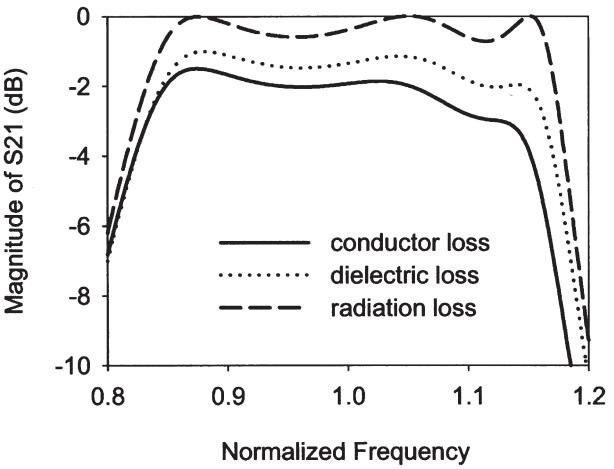

Figure 6 Simulated loss effects

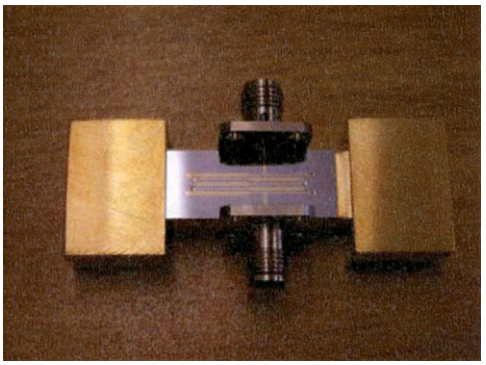

Figure 7 Fabricated SIR interdigital filter mount on brass test fixture. [Color figure can be viewed in the online issue, which is available at www.interscience.wiley.com]

extended stopband [6]. The ratio of high to low impedance shifts first higher order resonance up to a higher frequency value.

4. FURTHER DEVELOPMENT WITH MICROMACHINING

The advantage with the use of silicon is the ability for future developments such as silicon under etching to reduce the size of the SIR filter further and integration with other RF MEMS components. For example, using bulk micromachining it is possible to

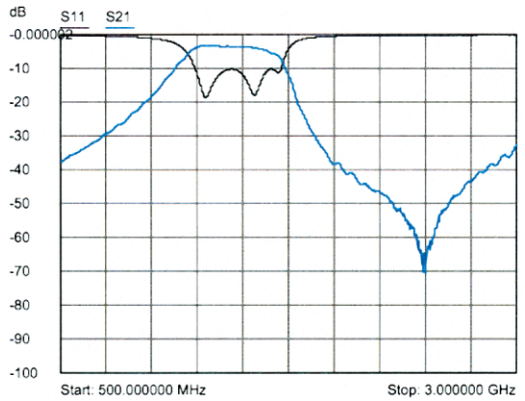

Figure 8 Measured UIR interdigital filter response. [Color figure can be viewed in the online issue, which is available at www.interscience.wiley.com]

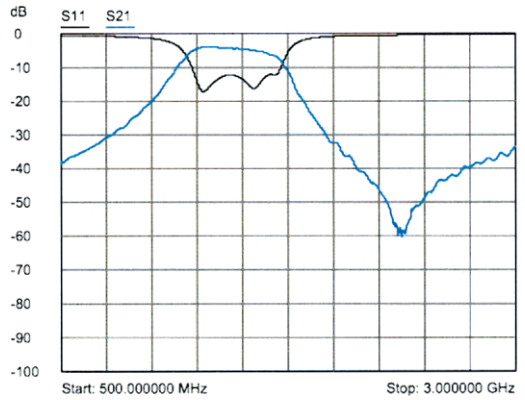

Figure 9 Measured SIR interdigital filter response. [Color figure can be viewed in the online issue, which is available at www.interscience.wiley.com]

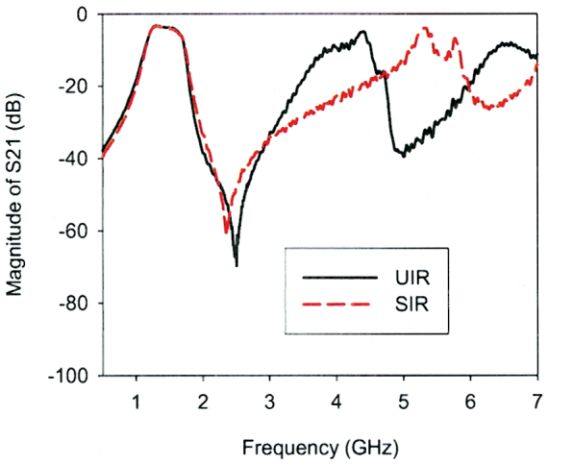

Figure 10 Measured wideband response for UIR and SIR designs. [Color figure can be viewed in the online issue, which is available at www.interscience.wiley.com]

reduce the thickness of the silicon substrate under the capacitive element of the SIR. The ground plane metal is then profiled to the change in thickness of the substrate as shown in Figure 11. The result is an increase in the capacitance of the element, which leads to a larger ratio of high to low impedance and reduce the length of the SIR. For the demonstration, simulations have been carried out to investigate the possible size reduction. The results of the initial investigation are shown in Table 5, with up to a 40% reduction in overall resonator length. Q measurements were also taken, showing very little reduction in performance of the resonator.

5. CONCLUSION

This article has demonstrated the design and construction of two wideband interdigital band pass filters with good test result both in simulation and measurement. The SIR filter design demonstrated the possible reduction in size over the UIR design with a small degradation in performance. The fabrication process was a success providing good via contacts with the micromachining and metal-

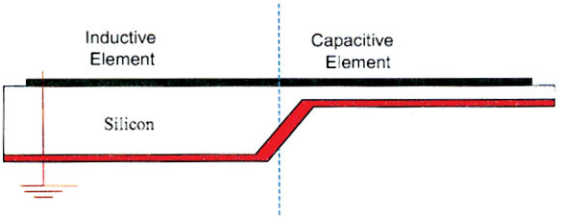

Figure 11 Micromachining below capacitive element of the SIR. [Color figure can be viewed in the online issue, which is available at www.interscience.wiley.com]

TABLE 5 Simulated Results of Micromachining Below Capacitive Element of the SIR

Thickness of Silicon Under Capacitive Element (μm)	Resonate Length at 1.5 GHz (mm)	Percentage reduction in size (%)
525	17.6	
300	15.0	14.8
200	13.5	23.3
100	10.5	40.3

lization of the vias. Using a flash of gold on the aluminium ground plane provided the low resistance contact to the test housing. The use of silicon micromachining has enabled these devices to be produced on a small scale. Integration with other devices on silicon can now be realized; further development in further reducing the size with bulk micromachining the silicon dielectric has also been proposed.

ACKNOWLEDGMENT

The authors thank Colin Bird and his industrial sponsor Selex Airborne systems. They also thank Robert Greed at BAE Systems ATC for continued help and BAE ATC at Filton in Bristol for the fabrication of the filters.

REFERENCES

1. G.L. Matthaei, Interdigital band-pass filters, Proc IRE, New York, NY (1962), 479–491.
2. J.S. Hong and M.J. Lancaster, Microstrip filters for RF/microwave applications, Wiley, New York, NY 2001.
3. K. Ma and J. Ma, A miniaturized silicon-based ground ring guarded patch resonator and filter, IEEE Microwave Wireless Compon Lett 15 (2005), 478–480.
4. D.S. Yu and C.F. Cheng, Narrow-band band-pass filters on silicon substrates at 30 GHz, IEEE MTT-S, Fort Worth, TX (2004), 1467–1470.
5. M.J. Madou, Fundamentals of microfabrication, Section Edition, CRC Press, Chapter 4.
6. H.-K. Pang, K.-M. Ho, K.-W. Tam, and R.P. Martins, A compact microstrip λ/4-SIR interdigital bandpass filter with extended stopband, IEEE MTT-S Dig, Fort Worth, TX (2004), 1621–1625.

SUBSTRUCTURING APPROACH TO OPTIMIZATION OF MATCHING FOR PHOTONIC CRYSTAL WAVEGUIDES

Ben Z. Steinberg, Amir Boag, and Orli Hershkoviz
School of Electrical Engineering
Tel Aviv University
Tel Aviv 69978, Israel

Received 2 March 2006

ABSTRACT: *A substructuring approach for numerical optimization of photonic crystal devices is proposed and demonstrated. Specifically, we consider the matching of coupled cavity waveguides (CCW's)—known also as coupled resonators optical waveguides (CROWs)—to free space. In this approach, one separates a priori between the invariant main structure that consists most of the PhC and the CCW, and the substructure that consists of a small portion of the CCW and evolves along the optimization course. Specific examples of matching configurations with insertion loss as low as few percent are presented.* © 2006 Wiley Periodicals, Inc. Microwave Opt Technol Lett 48: 1866–1871, 2006; Published online in Wiley InterScience (www.interscience.wiley.com). DOI 10.1002/mop.21766

Key words: *photonic crystals; guided waves; coupled cavity waveguide; coupled resonator optical waveguide-CROW; resonators*

1. INTRODUCTION

Photonic crystals (PhC) have a great potential for applications in optical devices [1]. Owing to their relatively high manufacturing costs, it is vital to have precise design tools that can simulate device configurations, predict their performance for a wide range of parameters, and obtain the optimal parameters that yield best performance. The purpose of this work is to develop an approach to optimize the matching of PhC waveguides to external structures, and to apply this approach to match a PhC-based coupled-cavity waveguide (CCW) [2, 3] to free space. Preliminary results have been reported in Ref. 4 and 5. Generally, in its PhC realization, the CCW comprises a linear array of widely-separated, equally-spaced, and identical microcavities in a photonic crystal. Each microcavity is manifested by a local defect that can localize light at a frequency within the original photonic band gap [1, 3]. A 2D example of a PhC comprising dielectric cylinders in a homogeneous background is shown in Figure 1. In this example, the microcavities are created by removing the corresponding dielectric cylinders. The waveguiding mechanism is based on tunneling of light between adjacent microcavities. The CCW constitutes a narrow-band low group velocity guiding structure, as opposed to a more common photonic crystal waveguide obtained by creating a contiguous line of defects, which supports a relatively wide-band guiding of optical signals [1]. The CCW central frequency is determined by the nature of its basic building block—the local defect, while the CCW bandwidth and group velocity are determined by the intercavity spacing [2, 3]. Because of these properties, this device is potentially an ideal candidate for optical communication tasks such as optical filtering and routing, optical delay lines [6], and optical parametric amplifiers [7]. Furthermore, it has recently been shown that the CCW can also be used to design ultra-compact optical gyroscopes [8].

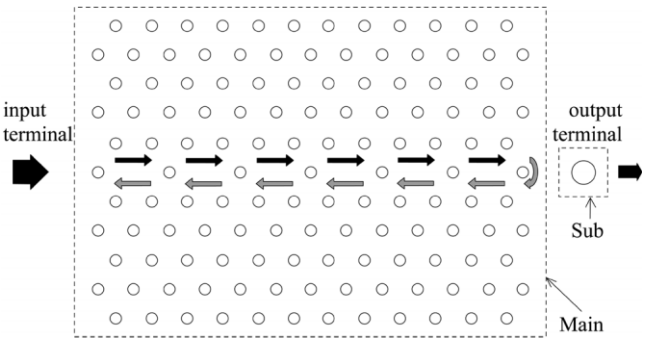

Figure 1 Transmission in photonic crystal coupled cavity waveguide

Clearly, the ability to match the CCW to the medium or structure surrounding the photonic crystal plays a pivotal role in using this device for the applications discussed above. The design of a matching structure can be formulated as an optimization problem: find the geometry of the output port that minimizes the back-reflections at the CCW terminal—see Figure 1. In recent years attention has been devoted to the problem of optimization of various aspects of photonic crystal devices [9–11]. Especial effort was also devoted to the problem of transmission through sharp bends [12–14]. Topology optimization [15] together with the moving asymptotes method [16] was used for optimization of bends [17, 18], T-junction [19], and termination of PhC waveguide [20]. A typical method for photonic crystal optimization comprises adding or removing cylinders or holes inside the photonic crystal and changing their radii or locations. This method was successfully applied for optimization of bends [14, 21, 22] and Y-junction [9]. Other works validated this technique in terms of transmission line theory [23] and used it for matching a finite length photonic crystal waveguide. Stochastic optimization methods based on the geometric modifications were also adapted for photonic crystal optimization. T-junction [11] was optimized using a genetic algorithm. Simulated annealing was used for bend optimization [10]. How-